Wind-Tunnel Boundary Interference on a V/STOL Model

CHING-FANG LO*
ARO Inc., Arnold Air Force Station, Tenn.

The wind-tunnel boundary interference on a V/STOL model is calculated in a test section with solid vertical and slotted horizontal walls. The method in the theory is the image method in addition to Fourier transforms with an equivalent homogeneous boundary condition on the slotted wall. The value of slot opening for zero interference is found as a function of model wake angle. The axial variation of the upwash interference suggests that certain variable slot widths in the stream direction will give zero upwash interference along the length of the test section.

Nomenclature

a = width of slot
A = cross-sectional area of model
A_1,A_2,B_1,B_2 = coefficients in Eq. (28)
b = semiwidth of test section
C = cross-sectional area of test section
h = semiheight of test section
K = geometric slot parameter, Eq. (7)
l = slot spacing
p_m = $(m^2\pi^2/b^2 + q^2)^{1/2}$
P = slot parameter, $(1 + K/h)^{-1}$
q = Fourier transform parameter
r = distance from element of surface of a vortex ring to field point P
s = distance from rotor disk to vortex ring
u = streamwise velocity
U = freestream velocity
w = upwash velocity
w_0 = induced velocity at rotor disk, $(\frac{1}{2})(d\Gamma/ds)$
x,y,z = Cartesian coordinates
α = angle of attack of rotor plane
β = effective skew angle, $\chi - \alpha$
Γ = circulation
δ_u = streamwise interference factor
δ_w = upwash interference factor
ζ = $s\cos\beta$
λ = height-to-width ratio
ξ = $s\sin\beta$
φ = perturbation velocity potential, $\varphi_i + \varphi_m$
φ_i = interference perturbation potential
φ_m = model perturbation potential
χ = skew angle

Subscripts

i = interference
m = model

Introduction

THE wind-tunnel test section for a V/STOL model, or model with high lift, is of great concern because of the lift interference. The high lift complicates the evaluation of the tunnel boundary interference because the wake associated with the model is at an angle to the horizontal plane, and in general, follows a curved path as it progresses downstream (Fig. 1). Furthermore, the intersection of the wake with the lower tunnel boundary makes the problem even more difficult, since the boundary condition in the vicinity of the intersection point is not very well understood.

In some recent investigations, a vortex lattice representation has been applied to calculate wall interferences.[1,2] The image method[3] and the Fourier transform method[4] have been used for tunnel interference calculations on a V/STOL model. The essential purposes of these theoretical calculations are 1) to provide a useful guide in selecting a minimum tunnel interference environment for V/STOL testing and 2) to provide a proper correction factor for tunnel testing data. Because of these two basic requirements a simplified model representing the flow model is adequate. This is the basic philosophy which has been followed in the wind-tunnel wall interference study.[5]

For most test sections considered in Heyson's report,[3] the interference varies widely with the skew angle between the wake and the vertical plane. However, for only an open lower boundary (i.e., the open boundary analog of ground effect), the wall interference has a small variation as a function of the skew angle. Thus, Wright[4] chooses a test section with solid upper wall, slotted vertical walls and open lower boundary. Since the open lower boundary may introduce oscillations of the test section flow, it should be replaced with a many-slotted lower boundary to prevent the oscillation, as suggested in Ref. 4.

The author's previous study[6] has shown that the lift interference for conventional models is insensitive to the porosity of the vertical walls for a tunnel height-to-width ratio less than 0.8. The theoretical calculations in Ref. 6 are based on a modification of the point-matching method with equivalent homogeneous boundary conditions of slotted walls. The experimental data have confirmed this conclusion for the slotted-wall tunnel case.[7] Therefore, the solid vertical sidewalls may be chosen for experimental convenience, such as installation of visualization equipment. For such a test section, the proper slot opening in the horizontal walls for zero interferences with a horizontal wake model has been found theoretically as well as experimentally. Hence, the test section having solid vertical and slotted horizontal walls has been chosen for study in this paper. The method used to obtain boundary interference is the image method in conjunction with Fourier transforms. An image system, which consists of a row of images, is introduced to satisfy boundary conditions on the solid vertical walls. Fourier transforms are then applied to solve the problem.

The purpose of the present investigation is to seek some test section configuration which may be expected to give small lift interference for a V/STOL model. In order to make the theory tractable, certain assumptions must be made in the analysis, such as an ideal model of the wake, the homogeneous boundary conditions of the slotted walls, etc. However, the

Received December 12, 1969; presented as Paper 70-575 at the AIAA 5th Aerodynamic Testing Conference, Tullahoma, Tenn., May 18–20, 1970; revision received May 25, 1970. The research reported herein was sponsored by the Arnold Engineering Development Center, Air Force Systems Command, under Contract No. AF40600-69-C-0001 with ARO Inc. Further reproduction is authorized to satisfy needs of the U. S. Government.

* Research Engineer, Propulsion Wind Tunnel Facility. Member AIAA.

theory should serve as a guide for choosing the slot configuration for experimental investigations in the development of an optimum test section for V/STOL model testing.

Representation of a Test Model

A V/STOL model can be represented by a rotor, lifting fan, or lifting jet. The disturbance potential of a rotor, lifting fan, or lifting jet is represented herein by an elliptic vortex cylinder sheet. For the small model assumption, corresponding to a wing with a vanishingly small span, the vortex cylinder may be replaced by a doublet line. Even for a small model, the usual small disturbance assumption is violated in the neighborhood of the wake intersection with the lower wall of the test section. However, if the wake is deflected only slightly below the horizontal, it intersects the lower boundary so far away from the model that the effect in the vicinity of the model may be negligible, even though the assumed boundary conditions are violated.

Among the V/STOL models chosen in the previous investigations, Heyson[3] assumes that the wake flows in a straight line intersecting the lower boundary at some point behind the model and then flows along the floor. Wright[4] uses a similar assumption except that the wake is assumed to break through the lower boundary and to have no further influence on the flowfield.

A jet in a cross-flow stream which may represent the model wake has two main features. First, the path of the wake is curved and depends primarily upon the initial jet velocity to the freestream velocity ratio and the initial jet deflection angle. Many experimental data, empirical equations and theoretical calculations are available for the prediction of the wake path (see Ref. 8). A sketch of the jet wake path shown in Fig. 1 is from Margason[8] and a straight line path used in Heyson's and Wright's theories[3,4] is also shown in Fig. 1. Second, the strength of the jet is decreased rapidly as the jet progresses downstream because of the mixing process between the jet and the freestream. Some of the previous experimental results[9] concerning the decay of axial velocity are shown in Fig. 2. Since the strength of the jet is directly proportional to the axial velocity parameter, Heyson's model with a constant wake strength from the model toward infinity downstream may be sketched in Fig. 2. In addition, Wright's model with a constant wake strength is also shown in Fig. 2 starting at the model and extending only to the lower tunnel wall. By comparing these two models with the real wake, it seems reasonable to choose Wright's model for the present study. However, the calculation could be extended to the curved wake with variable wake strength provided the relation between the wake strength and the axial velocity is known.

The rotor is assumed to be mounted at the center of the test section and its coordinates are shown in Fig. 3. If the rotor disk makes an angle of attack α with freestream velocity U and the vortex cylinder is swept downstream by a skew

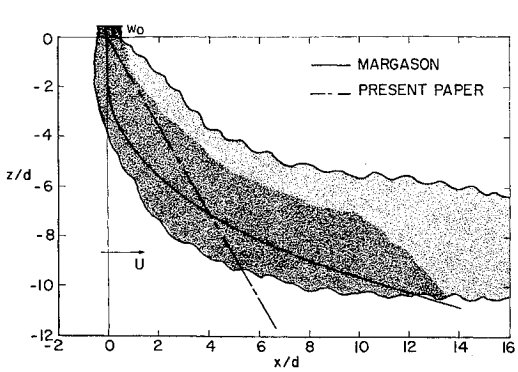

Fig. 1 Jet wake path for nozzle exiting downward at the jet-to-freestream velocity ratio, $w_0/U = 4.72$ (Ref. 8).

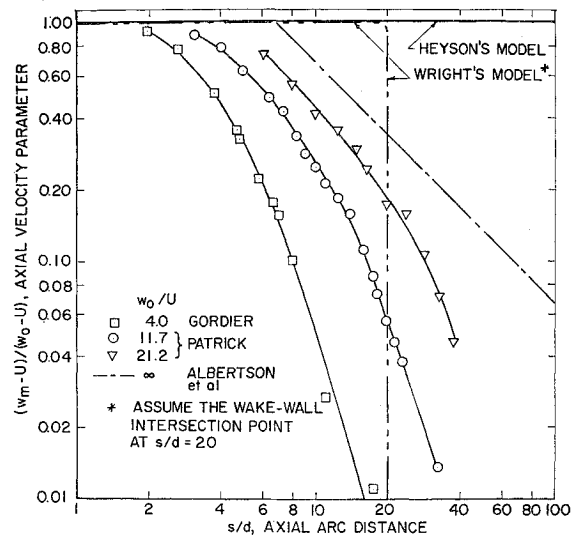

Fig. 2 Axial velocity decay of a jet in a cross flow (Ref. 9).

angle χ, then the axis of the vortex cylinder makes an angle $\beta = \chi - \alpha$ with the vertical, as shown in Fig. 3. The vortex sheet is made up of a continuous constant-strength distribution of circular vortex rings lying in planes parallel to the rotor plane. The element of potential $d\varphi_m$ at the field point P induced by the vortex ring of strength $(d\Gamma/ds)ds$ is expressed[10] as

$$d\varphi_m = (d\Gamma/ds)ds \iint (\cos\theta/4\pi r^2)dA \qquad (1)$$

where r is the distance from an element of surface of a vortex ring to the point P and s is the distance from the rotor disk to the vortex ring. Under the small model assumption, the variation of r over the surface 'A' enclosed by a vortex ring is small so that the angle θ between the vector area $\bar{A}$ and the vector distance $\bar{r}$ is constant. Hence, the integration of Eq. (1) becomes

$$d\varphi_m = (d\Gamma/ds)ds\ (A\ \cos\theta/4\pi r^2) \qquad (2)$$

This expression may be written in terms of x, y, z, and s by

$$r^2 = (x - \xi)^2 + y^2 + (z + \zeta)^2$$

$$\cos\theta = \bar{A}.\bar{r}/Ar = [(x - \xi)\sin\alpha + (z + \zeta)\cos\alpha]/r$$

where $\xi = s\sin\beta$, $\zeta = s\cos\beta$.

It follows that

$$d\varphi_m = A(d\Gamma/ds)ds[(x - \xi)\sin\alpha + (z + \zeta)\cos\alpha]/4\pi r^3 \qquad (3)$$

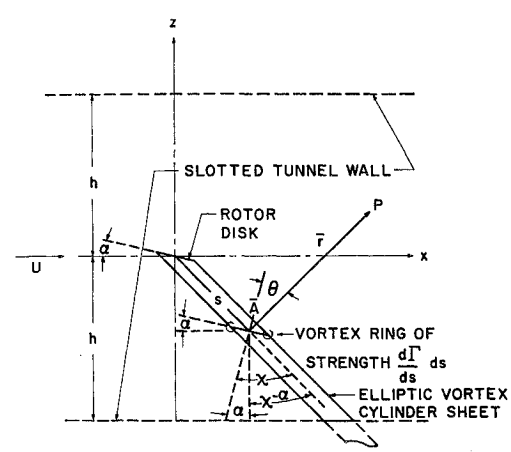

Fig. 3 Mathematical representation of a V/STOL model.

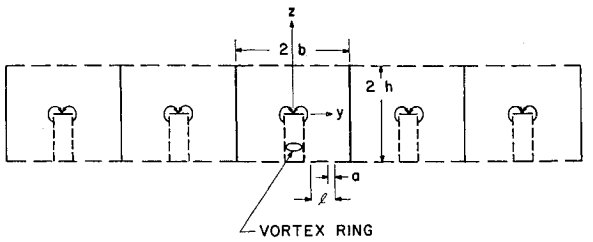

Fig. 4 Image system for satisfying boundary condition on solid vertical walls.

In free air, the vortex cylinder extends far below the lifting rotor. In the wind tunnel, however, each vortex ring representing the rotor wake is summed from the model to the intersection of the wake and the lower boundary which is the primary portion contributing to the interference. Hence, the disturbance potential becomes

$$\varphi_m = \int d\varphi_m = \int_0^{s_0} A(d\Gamma/ds)ds[(x-\xi)\sin\alpha + (z+\zeta)\cos\alpha]/4\pi r^3 \tag{4}$$

where s_0 is the distance from the rotor to the wake-wall intersection point along the wake path.

Boundary Condition of Test Section

As previously stated, the tunnel geometry to be studied consists of solid vertical walls and slotted horizontal walls.

For the solid vertical wall having no flow through the wall, the boundary condition may be expressed as

$$\partial\varphi/\partial y = 0 \quad \text{at} \quad y = \pm b \tag{5}$$

An equivalent boundary condition for slotted horizontal walls is

$$\varphi \pm K(\partial\varphi/\partial z) = 0 \quad \text{at} \quad z = \pm h \tag{6}$$

where K is related to the slot geometry by

$$K = (l/\pi)\ln[\csc(\pi a/2l)] \tag{7}$$

and a/l is the open area ratio as shown in Fig. 4. The geometric slot constant K may also be related to the wall porosity a/l by $K = [(l-a)/2]\tan[\pi(1-a/l)/2]$ as in Ref. 13. This gives a good correlation between theoretical results and experimental data obtained in our wind-tunnel development program. A slot parameter is introduced as $P = (1 + K/h)^{-1}$ where the value of $P = 0$ corresponds to a closed wall and $P = 1$ to an open wall.

Analysis

The field equation of an inviscid, incompressible fluid in terms of the velocity potential function Φ is Laplace's equation. In terms of the perturbation velocity potential φ and the uniform freestream velocity U the potential is

$$\Phi = Ux + \varphi \tag{8}$$

The linearity of the field equation and its boundary conditions permits the perturbation potential to be composed of two parts as

$$\varphi = \varphi_m + \varphi_i \tag{9}$$

where φ_m = the disturbance potential caused by a rotor and φ_i = the interference potential induced by the tunnel walls. Since the disturbance potential for a rotor is a series of vortex rings which satisfy Laplace's equation, the differential equation for the interference potential is again given by

$$(\partial^2/\partial x^2 + \partial^2/\partial y^2 + \partial^2/\partial z^2)\varphi_i = 0 \tag{10}$$

The solution of this equation associated with the boundary conditions, Eqs. (5) and (6), is obtained by the image method in conjunction with Fourier transforms. An image system which consists of a row of images, shown in Fig. 4, is introduced to satisfy boundary conditions on solid vertical walls. The expression of such an image system may be written from Eq. (4)

$$\varphi_r = \int_0^{s_0} A\left(\frac{d\Gamma}{ds}\right)ds \sum_{n=-\infty}^{\infty} \frac{[(x-\xi)\sin\alpha + (z+\zeta)\cos\alpha]}{4\pi r_n^3} \tag{11}$$

where $r_n = [(x-\xi)^2 + (y+2nb)^2 + (z+\zeta)^2]^{1/2}$.

In order to satisfy the boundary condition at the slotted walls, Eq. (6), an additional potential φ_s is required. The interference potential is given by

$$\varphi_i = \varphi_s + (\varphi_r - \varphi_m) \tag{12}$$

By substituting Eq. (12) in Eqs. (10), (5), and (6), the field equation and boundary conditions for φ_s are obtained.

$$(\partial^2/\partial x^2 + \partial^2/\partial y^2 + \partial^2/\partial z^2)\varphi_s = 0 \tag{13}$$

and

$$\partial\varphi_s/\partial y = -\partial\varphi_r/\partial y = 0 \quad \text{at} \quad y = \pm b \tag{14}$$

$$\varphi_s \pm K(\partial\varphi_s/\partial z) = -[\varphi_r \pm K(\partial\varphi_r/\partial z)] \quad \text{at} \quad z = \pm h \tag{15}$$

The successive application of Fourier transforms and finite Fourier transforms will give the solution of φ_s. First, the exponential Fourier transforms on $(x-\xi)$ with transform parameter q are applied to the differential equation and its boundary conditions, Eqs. (13–15). The equations in the transformed plane become

$$(\partial^2/\partial y^2 + \partial^2/\partial z^2 - q^2)\bar{\varphi}_s = 0 \tag{16}$$

and

$$\partial\bar{\varphi}_s/\partial y = 0 \text{ at } y = \pm b \tag{17}$$

$$\bar{\varphi}_s \pm K(\partial\bar{\varphi}_s/\partial z) = -[\bar{\varphi}_r \pm K(\partial\bar{\varphi}_r/\partial z)] \quad \text{at} \quad z = \pm h \tag{18}$$

where

$$\bar{\varphi}_s = (2\pi)^{-1/2}\int_{-\infty}^{\infty} \varphi_s(x-\xi)e^{iq(x-\xi)}\,d(x-\xi) \tag{19}$$

$$\bar{\varphi}_r = (2\pi)^{-1/2}\int_{-\infty}^{\infty} \varphi_r e^{iq(x-\xi)}\,d(x-\xi) = \frac{A(d\Gamma/ds)}{2\pi(2\pi)^{1/2}}\int_0^{s_0} ds \sum_{n=-\infty}^{\infty}\left[-i(\sin\alpha)\,qK_0(q\rho) + (\cos\alpha)q(z+\zeta)\frac{K_1(q\rho)}{\rho}\right] \tag{20}$$

$$\rho = [(y+2nb)^2 + (z+\zeta)^2]^{1/2}$$

$$q > 0$$

Since $\bar{\varphi}_r$ is an even function of y, the finite Fourier cosine transforms on the variable y are taken for Eqs. (16) and (18). By using Eq. (17), the following equations result

$$[\partial^2/\partial z^2 - (m^2\pi^2/b^2 + q^2)]\langle\bar{\varphi}_s\rangle = 0 \tag{21}$$

and

$$\langle\bar{\varphi}_s\rangle \pm K(\langle\partial\bar{\varphi}_s\rangle/\partial z) = -\langle\bar{\varphi}_r\rangle \pm K(\langle\partial\bar{\varphi}_r\rangle/\partial z) \quad \text{at} \quad z = \pm h \tag{22}$$

where

$$\langle\bar{\varphi}_s\rangle = \int_0^b \bar{\varphi}_s \cos\left(\frac{m\pi y}{b}\right)dy \tag{23}$$

$$\langle\bar{\varphi}_r\rangle = \int_0^b \bar{\varphi}_r \cos\left(\frac{m\pi y}{b}\right) dy =$$

$$\frac{A(d\Gamma/ds)}{2\pi(2\pi)^{1/2}} \int_0^{s_0} ds[-i(\sin\alpha)qH_0 + (\cos\alpha)q\,(z+\zeta)H_1] \quad (24)$$

with

$$H_0 = (\pi/2)e^{-|z+\zeta|p_m}/p_m \quad (25)$$

$$H_1 = (\pi/2)e^{-|z+\zeta|p_m}/|z+\zeta| \quad (26)$$

$$p_m = (m^2\pi^2/b^2 + q^2)^{1/2} \quad (27)$$

The evaluation of Eq. (24) has been shown by Acum.[11] The solution for Eq. (21) satisfying the boundary condition Eq. (22) is of the form

$$\langle\bar{\varphi}_s\rangle = \int_0^{s_0} ds\{[A_1\sinh(p_m\zeta) + iA_2\cosh(p_m\zeta)]\cosh p_m z + [B_1\cosh(p_m\zeta) + iB_2\sinh(p_m\zeta)]\sinh p_m z\} \quad (28)$$

A_1, A_2, B_1, and B_2 are functions of p_m listed as Eqs. (A1) to (A4) in the Appendix. The inversion of the transformed potential $\langle\bar{\varphi}_s\rangle$ from Eq. (28) yields

$$\varphi_s = (2\pi)^{-1/2} \int_{-\infty}^{\infty} \bar{\varphi}_s e^{-iq(x-\xi)}\, dq \quad (29)$$

where

$$\bar{\varphi}_s = \frac{1}{b}\sum_{m=0}^{\infty} j\,\langle\bar{\varphi}_s\rangle \cos\frac{m\pi}{b}\,y$$

$$j = \begin{cases} 1 & m = 0 \\ 2 & m \geq 1 \end{cases} \quad (30)$$

The interference velocities may then be obtained from the interference potential Eq. (12).

Interference Factors

The streamwise and upwash components of the interference factor for a rotor are expressed[4] as

$$\delta_u = (u_i/w_0)(C/A) \quad (31)$$

and

$$\delta_w = (w_i/w_0)(C/A) \quad (32)$$

respectively, where

u_i = boundary-induced interference velocity in stream direction
w_i = boundary-induced interference velocity in vertical direction, positive upward
w_0 = average velocity induced by lifting rotor at disk rotor, $(\frac{1}{2})(d\Gamma/ds)$
C = cross-sectional area of test section
A = area of rotor disk

The velocity in the stream or x direction may be obtained from Eqs. (4), (11), (12), and (29)

$$u_i = \partial\varphi_i/\partial x = (\partial\varphi_s/\partial x) + \partial(\varphi_r - \varphi_m)/\partial x \quad (33)$$

where

$$\frac{\partial\varphi_s}{\partial x} = \frac{1}{b(2\pi)^{1/2}}\frac{\partial}{\partial x}\int_{-\infty}^{\infty} dq \sum_{m=0}^{\infty} j\langle\bar{\varphi}_s\rangle \cos\frac{m\pi y}{b}\, e^{-iq(x-\xi)}$$

$$\frac{\partial(\varphi_r - \varphi_m)}{\partial x} = \frac{Aw_0}{2\pi}\sum_{n=-\infty}^{\infty} n \neq 0 \int_0^{s_0} ds \times \left[\frac{r_n^2 - 3(x-\xi)^2}{r_n^5}\sin\alpha - 3\,\frac{(x-\xi)(z+\zeta)}{r_n^5}\cos\alpha\right]$$

The velocity in the z direction is

$$w_i = \partial\varphi_i/\partial z = (\partial\varphi_s/\partial z) + \partial(\varphi_r - \varphi_m)/\partial z \quad (34)$$

where

$$\frac{\partial\varphi_s}{\partial z} = \frac{1}{b(2\pi)^{1/2}}\frac{\partial}{\partial z}\int_{-\infty}^{\infty} dq \sum_{m=0}^{\infty} j\langle\bar{\varphi}_s\rangle \cos\frac{m\pi y}{b}\, e^{-iq(x-\xi)}$$

$$\frac{\partial(\varphi_r - \varphi_m)}{\partial z} = \frac{Aw_0}{2\pi}\sum_{n=-\infty}^{\infty} n \neq 0 \int_0^{s_0} ds \times \left[\frac{-3(z+\zeta)(x-\xi)}{r_n^5}\sin\alpha + \frac{r_n^2 - 3(z+\zeta)^2}{r_n^5}\cos\alpha\right]$$

The summation of the effect of each vortex ring may be integrated with respect to s analytically. At the position of the model ($x = y = z = 0$), the velocity in the stream direction becomes

$$[u_i]_0 = [\partial\varphi_s/\partial x]_0 + [\partial(\varphi_r - \varphi_m)/\partial x]_0 \quad (35)$$

where $[\partial\varphi_s/\partial x]_0$ and $[\partial(\varphi_r - \varphi_m)/\partial x]_0$ are velocities induced by the slotted walls and solid walls, respectively. The expressions of these velocities are listed as Eqs. (A5) and (A6) of the Appendix. The upwash velocity at the position of the model becomes

$$[w_i]_0 = [\partial\varphi_s/\partial z]_0 + [\partial(\varphi_r - \varphi_m)/\partial z]_0 \quad (36)$$

where $[\partial\varphi_s/\partial z]_0$ and $[\partial(\varphi_r - \varphi_m)/\partial z]_0$ are as Eqs. (A7) and (A8) in the Appendix. The variation of the upwash velocity along the x axis is of the form, as $\alpha = 0$

$$[w_i]_{y=z=o} = [\partial\varphi_s/\partial z]_{y=z=o} + [\partial(\varphi_r - \varphi_m)/\partial z]_{y=z=o} \quad (37)$$

The expressions are listed as Eqs. (A9) and (A10) in the Appendix.

Numerical Results and Discussion

The interference factors of a V/STOL model are computed by numerical integration from Eqs. (35) and (36). It is shown in Fig. 5 that the upwash interference δ_w at the position of the model is a weak function of the angle-of-attack α within $-10° < \alpha < 20°$. Hence, results are presented herein only for zero angle-of-attack $\alpha = 0$.

The variations of the upwash interference factor δ_w and the streamwise interference factor δ_u at the position of the model, with wake skew angle β for various values of the slot parameter for the horizontal walls P_h are shown in Figs. 6 and 7,

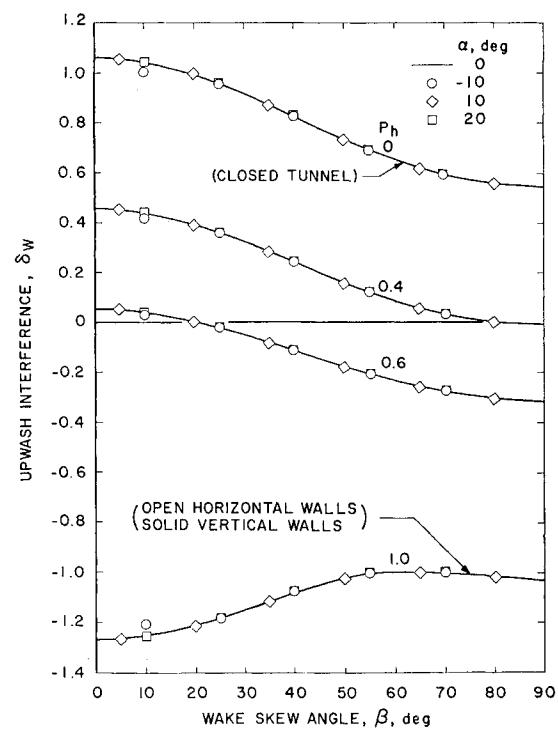

Fig. 5 Upwash interference at the position of the model for various angle-of-attack of rotor disk, h/b = 0.5.

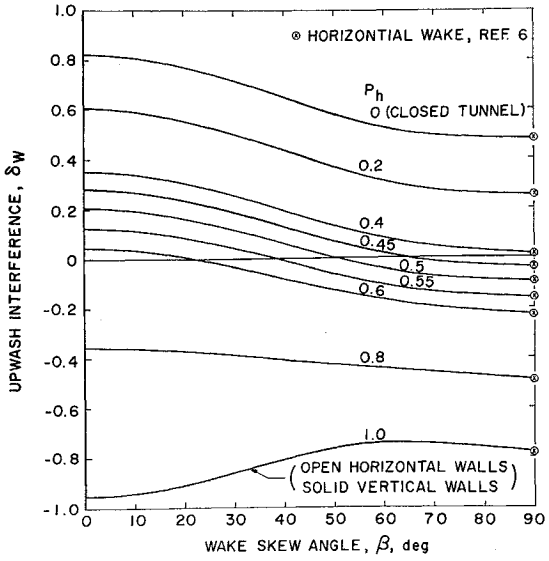

Fig. 6 Upwash interference factor at the position of the model ($x = y = z = 0$), $h/b = 0.667$, $\alpha = 0$.

respectively. The value of $P_h = 0$ corresponds to solid walls, $P_h = 1.0$ to open walls. In the limiting case of the rotor having a large forward velocity $\beta = 90°$, the upwash factor δ_w is related to the upwash factor for wings[4] as $\delta_w = 4\delta_0$. The constant factor of 4 is due to the difference in definition. The wing upwash factor δ_0 from Ref. 6 is also shown in Fig. 6. The results presented in Fig. 6 indicate that for zero upwash interference, the slot parameter P_h should increase from about 0.42 for the horizontal wake ($\beta = 90°$) to about 0.62 for a wake normal to the wall ($\beta = 0$). As can be seen in Fig. 7, for zero streamwise interference, the parameter P_h ranges from 0 to 0.8 as the skew angle varies from 90° to 0°.

The axial variation of the upwash interference factor for a specific slot parameter is calculated from Eq. (37) and shown in Fig. 8 for various values of skew angle. Figure 9 shows the axial variation of the upwash interference factor at specific values of skew angle for various values of the slot parameter. The results indicate that to obtain zero interference throughout the length of the test section, and hence zero pitching moment interference, a variable slot width is required in the longitudinal axis with the maximum width in the vicinity of the wake-wall intersection point.

Concluding Remarks

It is found that the test section having solid vertical and slotted horizontal walls chosen for the present study has zero upwash and streamwise interference at different values of slot opening for each wake skew angle. However, the upwash interference does not vary greatly with the wake skew angle. Moreover, for a proper value of slot opening, the variation of the upwash interference along the tunnel centerline is small. The result suggests that a variable slot width in the stream direction will provide a negligible amount of wall interference along the length of test section. On the other

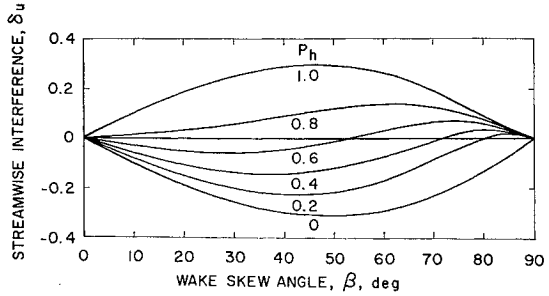

Fig. 7 Streamwise interference factor at the position of the model ($x = y = z = 0$), $h/b = 0.667$, $\alpha = 0$.

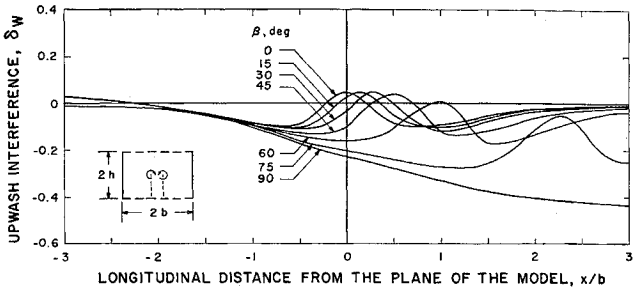

Fig. 8 Axial variation of the upwash interference factor, $h/b = 0.667$, $P_h = 0.60$, $\alpha = 0$.

hand, it seems helpful for correction simulation to vary the spanwise distribution of slot porosities from the physical consideration. However, by using a uniform spanwise distribution of slots, the wall configuration has the advantage to be applied to the multiple jet V/STOL models.

It should be noted that the boundary condition used in the theory is approximated by an equivalent condition. The effect of the complicated wake-wall intersection region is also neglected. Hence, the numerical value obtained for zero interference configuration should not be used directly to design slotted walls. Nevertheless, the theoretical result can serve as a guide in choosing slot configurations for an experimental investigation. In fact, a double tapered slot configuration inferred from the theoretical calculations is tested and the results indicate[7] that the configuration does eliminate the axial variation in lift interference for the tested range of jet-to-free-stream velocity ratios.

Another assumption in the theory is the straight line wake model which represents the essential feature for the case of a large skew-angle wake. A curved trajectory for the jet has been assumed for the interference calculation. Comparison of the curved and straight wake solutions shows[7] that the agreement between the two solutions is good if the zero interference configuration is chosen. This fact indicates that a wall configuration which produces zero lift interference is a weak function of jet path.

Finally, the present theory has been applied[12] to search a set of optimum wall configurations by varying the different porosities of the top and bottom walls. The experimental program will be continued along this direction.

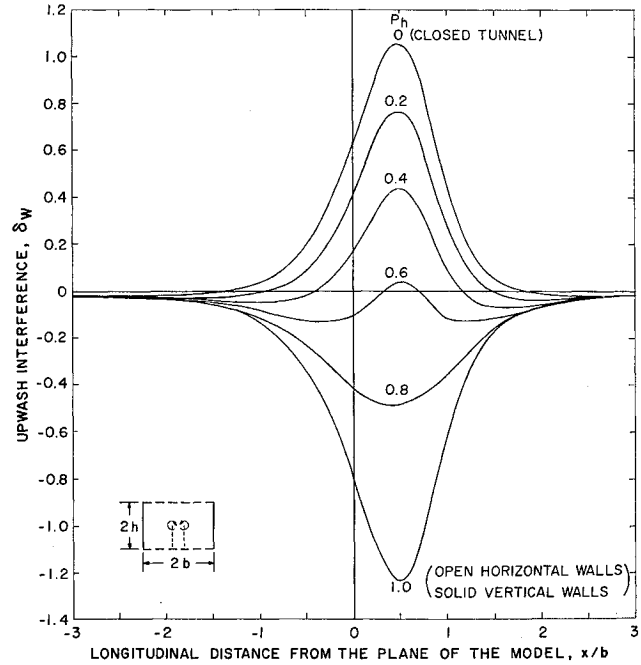

Fig. 9 Axial distribution of the upwash-interference factor for various porosities of the slotted horizontal walls, $h/b = 0.667$, $\beta = 45°$, $\alpha = 0$.

Appendix

The following expressions are for the coefficients A_1, A_2, B_1, and B_2 of Eq. (28):

$$A_1 = \frac{A(d\Gamma/ds)}{4(2\pi)^{1/2}} \frac{(1 - p_mK)\ (\cos\alpha)e^{-p_mh}}{\cosh p_mh + p_mK \sinh p_mh} \tag{A1}$$

$$A_2 = \frac{A(d\Gamma/ds)}{4(2\pi)^{1/2}} \frac{-q(1 - p_mK)\ (\sin\alpha)e^{-p_mh}}{p_m(\cosh p_mh + p_mK \sinh p_mh)} \tag{A2}$$

$$B_1 = \frac{A(d\Gamma/ds)}{4(2\pi)^{1/2}} \frac{-(1 - p_mK)\ (\cos\alpha)e^{-p_mh}}{\sinh p_mh + p_mK \cosh p_mh} \tag{A3}$$

$$B_2 = \frac{A(d\Gamma/ds)}{4(2\pi)^{1/2}} \frac{q(1 - p_mK)\ (\sin\alpha)e^{-p_mh}}{p_m(\sinh p_mh + p_mK \cosh p_mh)} \tag{A4}$$

The expressions for the streamwise interference velocity in Eq. (35) are of the form

$$\left[\frac{\partial\varphi_s}{\partial x}\right]_0 = \frac{1}{b}\left(\frac{2}{\pi}\right)^{1/2} \sum_{m=0}^{\infty} j \left\{\int_0^\infty A_1 \frac{q}{c^2 + d^2} [c \cosh p_mh \sin(qh \tan\beta) - d \sinh p_mh \cos(qh \tan\beta)]dq + \int_0^\infty A_2 \frac{q}{c^2 + d^2} [c \sinh p_mh \cos(qh \tan\beta) + d \cosh p_mh \sin(qh \tan\beta)]dq\right\} \tag{A5}$$

with

$$c = p_m \cos\beta \quad d = q \sin\beta$$

$$\left[\frac{\partial(\varphi_r - \varphi_m)}{\partial x}\right]_0 = \frac{Aw_0}{b^2\pi} \sum_{n=1}^{\infty} \left\{\left[\frac{s_0}{(2n)^2 r_0} - \frac{s_0^3 \sin^2\beta}{(2n)^2 r_0^3}\right] \sin\alpha + \left[\frac{s_0^3}{(2n)^2 r_0^3} \sin\beta \cos\beta\right] \cos\alpha\right\}, \quad r_0 = [(2nb)^2 + s_0^2]^{1/2} \tag{A6}$$

The expressions for the upwash interference velocity in Eq. (36) are of the form

$$\left[\frac{\partial\varphi_s}{\partial z}\right]_0 = \frac{1}{b}\left(\frac{2}{\pi}\right)^{1/2} \sum_{m=0}^{\infty} j \left\{\int_0^\infty B_1 \frac{p_m}{c^2 + d^2} [d \cosh p_mh \sin(qh \tan\beta) + c \sinh p_mh \cos(qh \tan\beta)]\, dq - \int_0^\infty B_2 \frac{p_m}{c^2 + d^2} [-d \sinh p_mh \cos(qh \tan\beta) + c \cosh p_mh \sin(qh \tan\beta)]\, dq\right\} \tag{A7}$$

$$\left[\frac{\partial(\varphi_r - \varphi_m)}{\partial z}\right]_0 = \frac{Aw_0}{b^2\pi} \sum_{n=1}^{\infty} \left\{\frac{s_0^3}{(2n)^2 r_0^3} \sin\beta \cos\beta \sin\alpha + \left[\frac{s_0}{3} \frac{3(2n)^2 + 2s_0^2}{(2n)^2 r_0^3} - \frac{s_0^3 (\sin^2\beta - 2\cos^2\beta)}{3(2n)^2 r_0^3}\right] \cos\alpha\right\} \tag{A8}$$

The expression for the upwash velocity distribution along the x axis in Eq. (37) is of the form

$$\left[\frac{\partial\varphi_s}{\partial z}\right]_{y=z=0} = -\frac{Aw_0}{b\ 2\pi} \sum_{m=0}^{\infty} j \int_0^\infty p_m \frac{(1 - p_mK)e^{-p_mh}}{\sinh p_mh + p_mK \cosh p_mh} [N(q) \cos qx + M(q) \sin qx]dq \tag{A9}$$

where

$$M(q) = [q \sin\beta + p_m \cos\beta \sinh p_mh \sin(qh \tan\beta) - q \sin\beta \cosh p_mh \cos(qh \tan\beta)]/(c^2 + d^2)$$

$$N(q) = [p_m \cos\beta \sinh p_mh \cos(qh \tan\beta) + q \sin\beta \cosh p_mh \sin(qh \tan\beta)]/(c^2 + d^2)$$

$$\left[\frac{\partial(\varphi_r - \varphi_m)}{\partial z}\right]_{y=z=o} = \frac{Aw_0}{\pi} [D(x) - 3E(x) \cos^2\beta] \tag{A10}$$

where

$$D(x) = \frac{1}{(x^2 + 4n^2b^2) - x^2 \sin^2\beta} \left[\frac{s_0 - x \sin\beta}{(r_0^2 + x^2 - 2xs_0 \sin\beta)^{1/2}} + \frac{x \sin\beta}{(x^2 + 4n^2b^2)^{1/2}}\right]$$

$$E(x) = \int_s^{s_0} \frac{s^2 ds}{[(x^2 + 4n^2b^2) - (2x \sin\beta)s + s^2]^{5/2}}$$

The integral $E(x)$ is integrable analytically.

References

[1] Joppa, R. G., "Wall Interference Effects in Wind Tunnel Testing of STOL Aircraft," *Journal of Aircraft*, Vol. 6, No. 3, May–June 1969, pp. 209–214.

[2] Kroeger, R. A. and Martin, W. A., 'The Streamline Matching Technique for V/STOL Wind Tunnel Wall Corrections," AIAA Paper 67-183, New York, 1967.

[3] Heyson, H. H., "Linearized Theory of Wind-Tunnel-Jet-Boundary Corrections and Ground Effect for VTOL-STOL Aircraft," TR R-124, 1962, NASA.

[4] Wright, R. H., "Test Section for Small Theoretical Wind-Tunnel-Boundary Interference on V/STOL Models," TR R-286, 1968, NASA.

[5] Garner, H. C. "Subsonic Wind Tunnel Wall Corrections," AGARDograph 109, Oct. 1966.

[6] Lo, C. F. and Binion, T. W., "A V/STOL Wind Tunnel Wall Interference Study," *Journal of Aircraft*, Vol. 7, No. 1, Jan.–Feb. 1970, pp. 51–57.

[7] Binion, T. W., Jr. and Lo, C.-F., "V/STOL Wind Tunnel Interferences with a High Disc Loading Model," AEDC TR (to be published).

[8] Margason, R. J., "The Path of a Jet Directed at Large Angles to a Subsonic Free Stream," TN D-4919, 1968, NASA.

[9] Patrick, M. A., "Experimental Investigation of the Mixing and Penetration of a Round Turbulent Jet Injected Perpendicularly into a Transverse Stream," *Transaction of the Institute of Chemical Engineers*, Vol. 45, 1967.

[10] Lamb, H., *Hydrodynamics*, 6th ed., Dover, New York, 1945, p. 212.

[11] Acum, W. E. A., "Note on the Evaluation of Solid-Blockage Corrections for Rectangular Wind Tunnels with Slotted Walls," ARC R&M 3297, National Physical Laboratory, Teddington, Middlesex, England.

[12] Lo, C.-F., "Test Section for a V/STOL Wind Tunnel," *Journal of Aircraft*, Vol. 7, No. 4, July–Aug. 1970, pp. 380–382.

[13] Chen, C. F. and Mears, J. W., "Experimental and Theoretical Study of Mean Boundary Conditions at Perforated and Longitudinally Slotted Wind Tunnel Walls," AEDC-TR-57-20, 1957, Arnold Engineering Development Center, Tenn.